Lossless Compression of Color Mosaic Images

Ning Zhang and Xiaolin Wu, *Senior Member, IEEE*

***Abstract*—Lossless compression of color mosaic images poses a unique and interesting problem of spectral decorrelation of spatially interleaved R, G, B samples. We investigate reversible lossless spectral-spatial transforms that can remove statistical redundancies in both spectral and spatial domains and discover that a particular wavelet decomposition scheme, called Mallat wavelet packet transform, is ideally suited to the task of decorrelating color mosaic data. We also propose a low-complexity adaptive context-based Golomb–Rice coding technique to compress the coefficients of Mallat wavelet packet transform. The lossless compression performance of the proposed method on color mosaic images is apparently the best so far among the existing lossless image codecs.**

***Index Terms*—Context quantization, entropy coding, digital camera, image compression.**

I. Introduction

MOST digital cameras use image sensors that sample only one of the three primary colors at each pixel position. Specifically, each pixel is covered with a filter and records just one of the three primary colors: red, green or blue. These primary color samples are interleaved in a two-dimensional (2-D) grid, or color mosaic, resembling a three-color checkerboard. The most popular single CCD color mosaic pattern is the one proposed by Bayer [1]. To reconstruct the true continuous-tone color, a procedure called color demosaicking is needed to interpolate the other two missing primary colors at each pixel. The image quality of digital cameras largely depends on the performance of the color demosaicking process.

Image data compression is an important component of digital camera design and digital photography. It is more than just an issue of saving storage and bandwidth, but rather to be considered in light of overall system performance and functionality, particularly in relation to color demosaicking. Currently, all digital cameras carry out color demosaicking prior to compression, apparently due to the considerations of easy user interface and device compatibility. However, industrial policy and standard issues aside, in our opinion, this design is suboptimal. Color demosaicking triples the amount of raw data by generating R, G, B bands via color interpolation. Ironically, the task of compression needs to decorrelate the three bands, which essentially attempts to reverse engineer the color interpolation process of demosaicking. This demosaicking-first and compression-later design unnecessarily increases algorithm complexity, reduces compression ratio, and burdens the on-camera I/O bandwidth.

In this paper, we propose to compress and store the color mosaic data directly, and perform demosaicking to reconstruct the R, G, B bands afterward, possibly offline. This relieves the camera from the tasks of color demosaicking and color decorrelation and also reduces the amount of input data to compression codec in the first place. The new workflow can potentially reduce on-camera computing power and I/O bandwidth. More importantly, the new design allows lossless or near-lossless compression of raw mosaic data, which is the main theme of this paper.

For many high-end digital photography applications, such as digital archiving of precious museum arts and relics, professional advertising, and digital cinema for which high image quality is paramount, it is crucial to have the original color mosaic data in lossless format. Our recent results in color demosaicking research [2] indicate that superior image quality can be obtained by more sophisticated color demosaicking algorithms than those implemented on camera, provided that original mosaic data are available. Furthermore, other image/video applications, such as super-resolution imaging and motion analysis, should also benefit from lossless compression of color mosaic data, in which even subpixel precision is much desired.

Lossless compression of mosaic color images poses a unique and interesting problem of spectral decorrelation (or more generally statistical modeling) of spatially interleaved R, G, B samples. Because a color mosaic image consists of interlaced R, G, B samples, existing decorrelation techniques such as DPCM, DCT, and wavelets may not work effectively by treating a mosaic image as a grayscale one. In this paper, we examine a number of interband coding techniques for lossless coding of color mosaic images. Our focus is on reversible lossless spectral-spatial transforms that can remove statistical redundancies in both spectral and spatial domains. Interestingly, we discover that a unique wavelet decomposition scheme, called the Mallat packet transform, is ideally suited to the task of decorrelating color mosaic data.

The presentation is organized as follows. Section II presents and evaluates some schemes of coding mosaic images by de-interleaving R, G, B samples prior to compression. In Section III, we consider an alternative approach of compressing color mosaic images directly without de-interleaving the color bands. We study the strength and weakness of both DPCM and wavelet-based lossless coding methods in the above two different approaches. Section IV offers a wavelet analysis of mosaic images. The analysis leads to a new wavelet decomposition scheme that is well suited for lossless coding of Bayer pattern mosaic data directly without de-interleaving. This new wavelet decomposition, which resembles the SPACL mode of JPEG 2000 standard,

Manuscript received September 29, 2004; revised April 18, 2005. This work was supported in part by the Natural Sciences and Engineering Research Council of Canada under the NSERC-DALSA Industrial Research Chair in Digital Cinema. The associate editor coordinating the review of this manuscript and approving it for publication was Dr. Giovanni Poggi.

The authors are with the Department of Electrical and Computer Engineering, McMaster University, Hamilton, ON L8K 4K1 Canada (e-mail: ningzhang@mail.ece.mcmaster.ca; xwu@ece.mcmaster.ca).

Digital Object Identifier 10.1109/TIP.2005.871116

has the nice property of decorrelating color samples both spatially and spectrally. Section V introduces a fast context-based Golomb–Rice coding scheme to compress the coefficients of the proposed wavelet transform. Section VI presents experimental results and Section VII concludes.

II. Deinterleaved Compression

Since most digital cameras use CCD sensor arrays of Bayer pattern, we are concerned with the lossless compression of color mosaic images of Bayer pattern, but the techniques to be developed in this paper can be generalized to other mosaic color sampling schemes. The Bayer color filter array and a resulting mosaic image are presented in Fig. 1.

Let $I_{(x,y)}$ be the color sample at pixel position (x, y), then the Bayer color mosaic pattern is defined by

$$I_{(x,y)} = \begin{cases} G_{(x,y)} & x-y \text{ is even} \\ R_{(x,y)} & x \text{ is odd, } y \text{ is even} \\ B_{(x,y)} & x \text{ is even, } y \text{ is odd.} \end{cases} \quad (1)$$

A natural way of compressing color mosaic images is to first deinterleave the three color channels, and then code each of the three down-sampled color channels individually. Specifically, the Bayer pattern

$$\begin{array}{cccccccc} G_{0,0} & R_{0,1} & G_{0,2} & R_{0,3} & G_{0,4} & R_{0,5} & G_{0,6} & R_{0,7} \\ B_{1,0} & G_{1,1} & B_{1,2} & G_{1,3} & B_{1,4} & G_{1,5} & B_{1,6} & G_{1,7} \\ G_{2,0} & R_{2,1} & G_{2,2} & R_{2,3} & G_{2,4} & R_{2,5} & G_{2,6} & R_{2,7} \\ B_{3,0} & G_{3,1} & B_{3,2} & G_{3,3} & B_{3,4} & G_{3,5} & B_{3,6} & G_{3,7} \\ G_{4,0} & R_{4,1} & G_{4,2} & R_{4,3} & G_{4,4} & R_{4,5} & G_{4,6} & R_{4,7} \\ B_{5,0} & G_{5,1} & B_{5,2} & G_{5,3} & B_{5,4} & G_{5,5} & B_{5,6} & G_{5,7} \\ G_{6,0} & R_{6,1} & G_{6,2} & R_{6,3} & G_{6,4} & R_{6,5} & G_{6,6} & R_{6,7} \\ B_{7,0} & G_{7,1} & B_{7,2} & G_{7,3} & B_{7,4} & G_{7,5} & B_{7,6} & G_{7,7} \end{array}$$

can be de-interleaved into the following three down-sampled color channels:

$$\begin{array}{cccccccc} G_{0,0} & & G_{0,2} & & G_{0,4} & & G_{0,6} & \\ & G_{1,1} & & G_{1,3} & & G_{1,5} & & G_{1,7} \\ G_{2,0} & & G_{2,2} & & G_{2,4} & & G_{2,6} & \\ & G_{3,1} & & G_{3,3} & & G_{3,5} & & G_{3,7} \\ G_{4,0} & & G_{4,2} & & G_{4,4} & & G_{4,6} & \\ & G_{5,1} & & G_{5,3} & & G_{5,5} & & G_{5,7} \\ G_{6,0} & & G_{6,2} & & G_{6,4} & & G_{6,6} & \\ & G_{7,1} & & G_{7,3} & & G_{7,5} & & G_{7,7} \end{array}$$

$$\begin{array}{cccc} R_{0,1} & R_{0,3} & R_{0,5} & R_{0,7} \\ R_{2,1} & R_{2,3} & R_{2,5} & R_{2,7} \\ R_{4,1} & R_{4,3} & R_{4,5} & R_{4,7} \\ R_{6,1} & R_{6,3} & R_{6,5} & R_{6,7} \end{array} \qquad \begin{array}{cccc} B_{1,0} & B_{1,2} & B_{1,4} & B_{1,6} \\ B_{3,0} & B_{3,2} & B_{3,4} & B_{3,6} \\ B_{5,0} & B_{5,2} & B_{5,4} & B_{5,6} \\ B_{7,0} & B_{7,2} & B_{7,4} & B_{7,6}. \end{array}$$

Let us develop a general framework for de-interleaved compression of mosaic images. First, we code the green channel before the other two channels, because the green channel has twice as many samples and, hence, higher intrachannel correlation. Once the green samples are coded, we utilize the interchannel correlation to compress red and blue channels, but one problem needs to be addressed. In the Bayer pattern, the green channel consists of a diamond grid (or so-called quincunx array), while all existing lossless image compression standards operate on

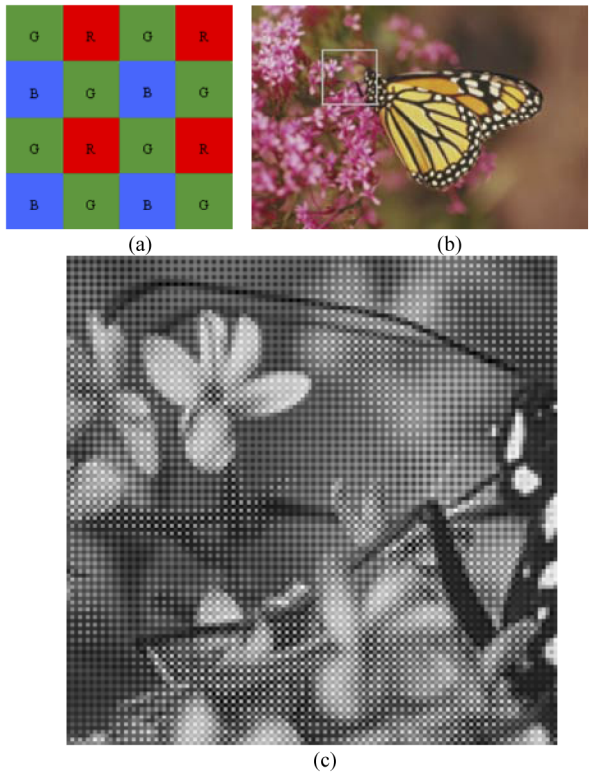

Fig. 1. Bayer pattern and an example of mosaic image: (a) Bayer color filter array; (b) an original color image: Monarch; (c) Bayer pattern mosaic image of the selected region in (b). (Color version available online at http://ieeexplore.ieee.org.)

square sample grid. We need to transform the green quincunx array to rectangular array in preparing it for compression. There are many ways of transforming or deinterleaving the diamond sample grid into a square sample grid. We examine the following four.

1) **Merge:** The quincunx array is converted to rectangular array by shifting all odd columns one pixel to the left and form

$$\begin{array}{cccc} G_{0,0} & G_{0,2} & G_{0,4} & G_{0,6} \\ G_{1,1} & G_{1,3} & G_{1,5} & G_{1,7} \\ G_{2,0} & G_{2,2} & G_{2,4} & G_{2,6} \\ G_{3,1} & G_{3,3} & G_{3,5} & G_{3,7} \\ G_{4,0} & G_{4,2} & G_{4,4} & G_{4,6} \\ G_{5,1} & G_{5,3} & G_{5,5} & G_{5,7} \\ G_{6,0} & G_{6,2} & G_{6,4} & G_{6,6} \\ G_{7,1} & G_{7,3} & G_{7,5} & G_{7,7}. \end{array}$$

2) **Reversible de-interlacer:**

$$\begin{array}{cccc} G_{0,0} & G_{0,2} & G_{0,4} & G_{0,6} \\ g_{1,1} & g_{1,3} & g_{1,5} & g_{1,7} \\ G_{2,0} & G_{2,2} & G_{2,4} & G_{2,6} \\ g_{3,1} & g_{3,3} & g_{3,5} & g_{3,7} \\ G_{4,0} & G_{4,2} & G_{4,4} & G_{4,6} \\ g_{5,1} & g_{5,3} & g_{5,5} & g_{5,7} \\ G_{6,0} & G_{6,2} & G_{6,4} & G_{6,6} \\ g_{7,1} & g_{7,3} & g_{7,5} & g_{7,7}. \end{array}$$

This scheme was proposed for lossy compression of Bayer pattern mosaic data [3], [4]. Odd column data are

passed through a vertical low-pass filter before merging with even columns, namely

$$g_{(x,y)} = \frac{1}{4}\left[(G_{(x-1,y-1)} + 2G_{(x,y)} + G_{(x-1,y+1)}\right]. \quad (2)$$

Since $g_{(x,y)}$ increases the dynamic range of G by one bit, the above transform becomes inefficient for lossless coding. In other words, if the binary representation of $G_{(x,y)}$ has N bits, $N+1$ bits are required to represent $g_{(x,y)}$ in order to have lossless inverse transform. Although $g_{(x,y)}$ and $G_{(x,y)}$ have the same dynamic range in (2), an extra bit is needed to resolve the parity of the sum for lossless reconstruction.

3) **Separation**

$$\begin{array}{cccc|cccc} G_{0,0} & G_{0,2} & G_{0,4} & G_{0,6} & G_{1,1} & G_{1,3} & G_{1,5} & G_{1,7} \\ G_{2,0} & G_{2,2} & G_{2,4} & G_{2,6} & G_{3,1} & G_{3,3} & G_{3,5} & G_{3,7} \\ G_{4,0} & G_{4,2} & G_{4,4} & G_{4,6} & G_{5,1} & G_{5,3} & G_{5,5} & G_{5,7} \\ G_{6,0} & G_{6,2} & G_{6,4} & G_{6,6} & G_{7,1} & G_{7,3} & G_{7,5} & G_{7,7}. \end{array}$$

4) Rotation

$$\begin{array}{ccccccc} & & & G_{0,0} & & & \\ & & G_{2,0} & G_{1,1} & G_{0,2} & & \\ & G_{4,0} & G_{3,1} & G_{2,2} & G_{1,3} & G_{0,4} & \\ G_{6,0} & G_{5,1} & G_{4,2} & G_{3,3} & G_{2,4} & G_{1,5} & G_{0,6} \\ G_{7,1} & G_{6,2} & G_{5,3} & G_{4,4} & G_{3,5} & G_{2,6} & G_{1,7} \\ & G_{7,3} & G_{6,4} & G_{5,5} & G_{4,6} & G_{3,7} & \\ & & G_{7,5} & G_{6,6} & G_{5,7} & & \\ & & & G_{7,7}. & & & \end{array}$$

After one of the above deinterleaving transforms, the green channel can be coded using any of the existing lossless image codecs, such as JPEG-LS and JPEG 2000 lossless mode. Table I lists the bit rates of the lossless image compression standards JPEG-LS [5] and JPEG-2000 [6] (lossless mode) on the outputs of three of the above deinterleaving transforms. In Table I, for each test image, the number in bold face represents the best result among all deinterleaving transforms. There is no single winning transform for all the images. Not surprisingly, the separation transform performs the worst on average because it disregards the correlation between the two resulting subimages of green samples. The compression results of the merge and rotation transforms are very close for a given lossless image codec. In our comparison study JPEG-LS achieves better lossless compression than JPEG-2000 on all test images for the de-interleaving methods of separation and merge. For the rotation method, we present only the results of JPEG-LS not those of JPEG 2000, because it is relatively easy to modify JPEG-LS to code the rotated image but very difficult to do the same with JPEG 2000.

Once the green channel is coded and made known to the decoder, it can be used as an anchor to facilitate the compression of red and blue channels by exploiting the spectral correlation. To this end, we estimate the missing green values from the existing green samples at the pixel positions where either red or blue sample is taken. We denote such estimates by $g_{(x,y)}$, where the value of $x-y$ is odd, to distinguish them from the existing green samples $G_{(x,y)}$, where the value of $x-y$ is even. Rather than code $R_{(x,y)}$ and $B_{(x,y)}$ separately, we losslessly code the two color difference images

$$\alpha_{(x,y)} = R_{(x,y)} - g_{(x,y)} \quad \text{and} \quad \beta_{(x,y)} = B_{(x,y)} - g_{(x,y)}. \quad (3)$$

Since the decoder can make the same estimates $g_{(x,y)}$ as the encoder, it can reconstruct the original $R_{(x,y)}$ and $B_{(x,y)}$ from $\alpha_{(x,y)}$ and $\beta_{(x,y)}$ without any loss. The difference images $\alpha_{(x,y)}$ and $\beta_{(x,y)}$, which can be regarded approximately as two chrominance components, are more compressible than $R_{(x,y)}$ or $B_{(x,y)}$ because they are typically low-pass signals due to the interchannel correlation. Furthermore, the color difference images $\alpha_{(x,y)}$ and $\beta_{(x,y)}$ provide vital information in many color demosaicing algorithms [1], [7]–[9]. Therefore, lossless coding of $\alpha_{(x,y)}$ and $\beta_{(x,y)}$ serves dual purposes of lossless compression of color mosaic data and color demosaicking.

In estimating the missing green samples $g_{(x,y)}$, we have evaluated various interpolation schemes, including bilinear interpolation, bi-cubic B-Spline [9] and some nonlinear methods [7], [8]. Table II lists the lossless bit rates of the red and blue mosaic samples obtained by three coding schemes: 1) intrachannel coding of red and blue; 2) color difference coding with bilinear green interpolation; 3) color difference coding with bi-cubic B-spline green interpolation. It is clear from Table II that coding color differences is more effective than coding the red and blue channels individually. The coding gain is more than 7.5% on average, which is a significant margin by the standard of lossless image coding. The precision of green interpolation can improve the lossless compression of color mosaic images, but only marginally. Simple bilinear interpolation works satisfactorily.

Table III presents the overall lossless bit rates of JPEG-LS and JPEG 2000 lossless mode on the de-interleaved green channel (using the merge deinterleaving transform) and the two color difference images $\boldsymbol{\alpha}$ and $\boldsymbol{\beta}$ with $\mathbf{g}$ being estimated by bilinear

TABLE I
LOSSLESS BIT RATES OF GREEN CHANNEL UNDER DIFFERENT DEINTERLEAVING TRANSFORMS WHILE BEING COMPRESSED BY JPEG-LS AND JPEG 2000

	Separation		Merge		Rotation
Image	J2K	JPEG-LS	J2K	JPEG-LS	JPEG-LS
Woman	5.251	5.207	5.167	5.086	**5.004**
Bike	5.374	5.029	5.237	4.944	**4.919**
Monarch	4.699	4.518	4.496	4.318	**4.166**
Wall	6.197	**5.943**	6.147	5.985	6.068
Boat	5.364	5.176	5.200	**5.031**	5.131
Windows	6.418	**6.060**	6.389	6.320	6.285
Landscape	6.815	6.585	6.635	**6.401**	6.434
Fence	5.201	5.078	5.094	5.075	**5.054**
Lighthouse	5.234	5.05	5.063	**4.896**	4.976
Average	5.617	5.405	5.492	5.340	**5.337**

TABLE II
LOSSLESS BIT RATES OF RED AND BLUE MOSAIC SAMPLES USING JPEG-LS

	Intra-channel		Bilinear Interpolation		CubicSpline Interpolation	
Image	R	B	R-g	B-g	R-g	B-g
Woman	5.185	5.273	4.751	4.792	**4.698**	**4.653**
Bike	4.812	5.254	**4.571**	5.003	4.647	**4.954**
Monarch	4.528	4.625	**4.323**	**4.334**	4.397	4.391
Wall	5.962	5.937	5.566	5.526	**5.421**	**5.343**
Boat	5.199	5.349	4.833	5.023	**4.726**	**4.912**
Windows	6.062	6.04	5.688	5.664	**5.505**	**5.501**
Landscape	6.594	6.531	6.085	6.138	**6.039**	**6.122**
Fence	5.118	5.051	4.713	4.774	**4.645**	**4.773**
Lighthouse	5.053	5.154	4.778	4.881	**4.752**	**4.854**
Average	5.390	5.468	5.034	5.126	**4.981**	**5.056**

TABLE III
LOSSLESS BIT RATES OF DEINTERLEAVED MOSAIC IMAGES BY JPEG-LS AND JPEG 2000

	No interpolation		Bilinear interpolation	
Image	JPEG-LS	JPEG-2K	JPEG-LS	JPEG-2K
Woman	5.158	5.220	4.929	4.968
Bike	4.989	5.289	4.866	5.064
Monarch	4.447	4.613	4.323	4.448
Wall	5.967	6.152	5.766	5.855
Boat	5.153	5.323	4.980	5.085
Windows	6.186	6.388	5.998	6.086
Landscape	6.482	6.697	6.256	6.406
Fence	5.080	5.154	4.909	4.926
Lighthouse	5.000	5.161	4.863	4.960
Average	**5.384**	**5.555**	**5.210**	**5.311**

interpolation. For comparison purposes, we also give the results of coding red and blue channels directly without interband decorrelation.

III. INTERLEAVED COMPRESSION

An alternative approach to lossless compression of color mosaic images is to process the mosaic data directly without de-interleaving the color channels. In other words, the compression algorithm pretends that the color mosaic image is a single-channel grrayscale image. This treatment has the advantage of simpler codec design and lower complexity than compression after de-interleaving. The simplest way is to apply a lossless image coding algorithm directly to raw color mosaic images without any preprocessing. For a quick assessment of different compression methods, when applied to mosaic images directly, the reader is referred to Table VI of Section VI (not placed here to save space) for the lossless bit rates of JPEG-LS and JPEG 2000 (using the 5-3 integer filter) standards on some common test images.

Interestingly, and somewhat surprisingly, JPEG-2000 outperforms JPEG-LS by a significant margin (more than 10%), when both applied to compress color mosaic images without de-interleaving. Recall from the proceeding section that the performance comparison between the two algorithms in the case of de-interleaved compression gave exactly opposite results. This reversal in relative coding efficiency is largely due to a fundamental difference in decorrelation mechanisms of the two algorithms: DPCM for JPEG-LS and lifting integer wavelet for JPEG 2000.

The DPCM scheme is suited to remove long term memory of a smooth signal in the spatial domain. It becomes ineffective on decorrelating mosaic images of periodic patterns. The energy of a mosaic image can be packed into the spatial-frequency domain of the wavelet far more efficiently than in the spatial domain. To expose this weakness of DPCM on mosaic images, in Fig. 2 we present the prediction residual images of JPEG-LS when being applied to a natural image [given in Fig. 6(a)] and its mosaic counterpart [given in Fig. 6(b)]. The DPCM residual signal of the mosaic image has significantly greater amplitude than that of the natural image. Moreover, the DPCM residuals still exhibit the original mosaic structure, with their statistics far from being i.i.d. In other words, the median predictor used by JPEG-LS fails to pack the signal energy and decorrelate the samples.

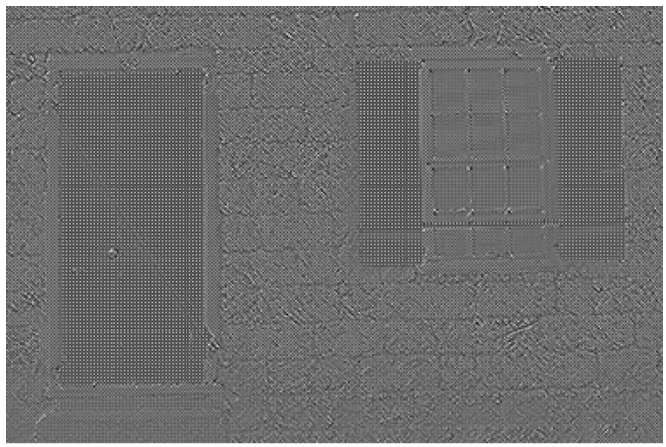

(a)

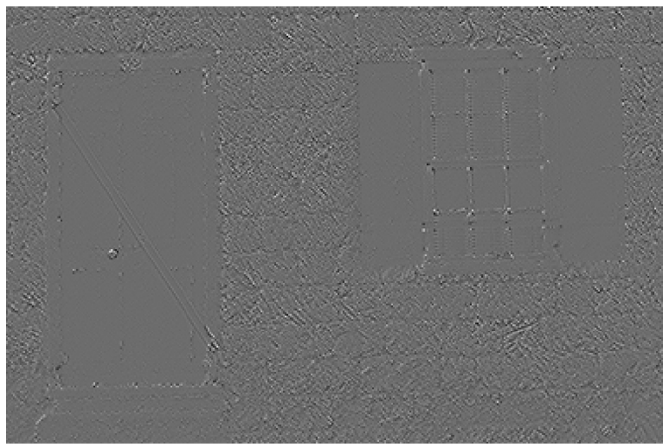

(b)

Fig. 2. Residual images of the median predictor of JPEG-LS (the mid-gray represents zero). (a) Residual image of Bayer mosaic image. (b) Residual image of the original green channel.

Let us compare in Fig. 3 the histograms of the prediction residual images Fig. 2(a) and Fig. 2(b) of JPEG-LS, for the mosaic image and the corresponding normal image, respectively. It is well known that the DPCM residuals of a normal image signal obey a Laplacian distribution, as being evident in Fig. 3(b), but this is no longer true for the DPCM residuals of a mosaic image. Note that the distribution of Fig. 3(a) is multimodal and asymmetric against the origin. The residuals of JPEG-LS for mosaic images deviate drastically from a Laplacian distribution, and they cannot even be modeled by a generalized Gaussian distribution. Unfortunately, the entropy code (Golomb–Rice code) of JPEG-LS assumes a Laplacian distribution of the prediction residuals. This severe mismatch between the model and the source also explains the poor performance of JPEG-LS on mosaic images. The problem will be corrected in the next two sections.

IV. WAVELET ANALYSIS OF MOSAIC IMAGES

In a sharp contrast to DPCM, the wavelet, being a tool of frequency–time analysis, can compactly characterize periodic color mosaic signals, as will be demonstrated by the analysis of this section. Based on the analysis, we propose a unique

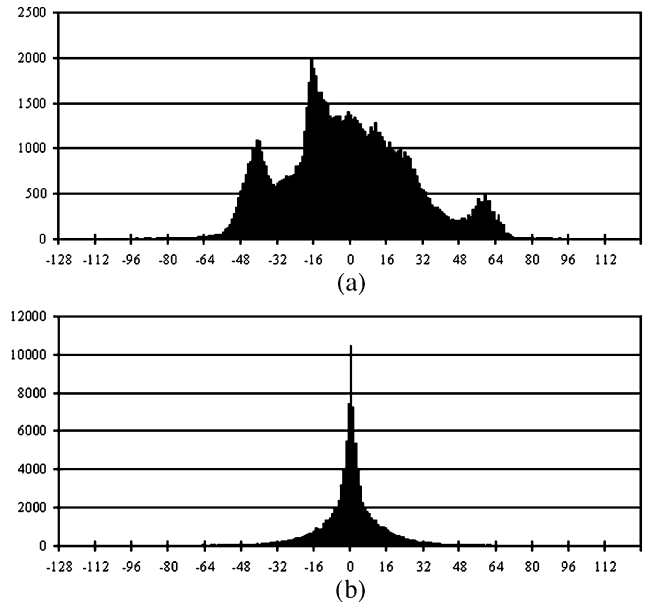

Fig. 3. Histograms of JPEG-LS residuals for mosaic image and the original green channel. (a) Histogram of the residual image in Fig. 2(a). (b) Histogram of the residual image in Fig. 2(b).

so-called Mallat packet wavelet transform for direct compression of mosaic images without de-interleaving. As we will see, the proposed wavelet transform simultaneously performs spatial and spectral decorrelation of color samples with a great ease and at a low cost.

Let us start by examining an interesting interplay between the Bayer pattern and the 2-D integer wavelet transform via separable one-dimensional (1-D) lifting. One level of the wavelet transform produces four subbands that have clear interpretations of the attributes of the Bayer color signal. As shown in Fig. 4, a 2-D wavelet transform (after decimation) and the Bayer pattern both have a 2×2 periodical sampling pattern. This correspondence makes 2-D wavelet transforms very efficient to represent the Bayer pattern in frequency–space domain. The effect of performing a 2-D wavelet transform on a mosaic image is illustrated by Fig. 5. In this example, the Bayer mosaic data of a uniform color image are transformed into four constant subbands, although the input mosaic image is, itself, a high-frequency signal.

We can explain the effect of Fig. 5 analytically using, for example, the 5-3 integer wavelet. Other wavelets, such as 9/7M, 5/11-C [10], behave similarly. The low- and high-pass filers of the 5-3 integer wavelet are

$$\mathbf{f}_L = \left(-\frac{1}{8}, \frac{1}{4}, \frac{3}{4}, \frac{1}{4}, -\frac{1}{8}\right) \quad \mathbf{f}_H = \left(-\frac{1}{2}, 1, -\frac{1}{2}\right). \tag{4}$$

After applying the 2-D low-pass filter $\mathbf{F}_{LL} = \mathbf{f}_L^T \mathbf{f}_L$ to the Bayer mosaic image, the LL subband can be interpreted as the luminance channel of the original full color image. In a window of smooth color, where red, green, and blue color components are approximately constants (i.e., $R_{(x,y)} \cong R$, $G_{(x,y)} \cong G$, $B_{(x,y)} \cong B$), the coefficients in the LL subband are

$$\frac{1}{4}(R + 2G + B).$$

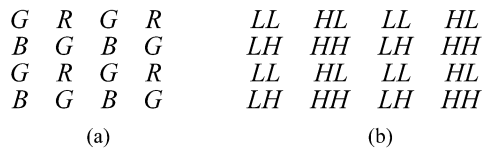

Fig. 4. The 2×2 periodical sampling pattern of (a) Bayer mosaic data and (b) 2-D wavelet transform.

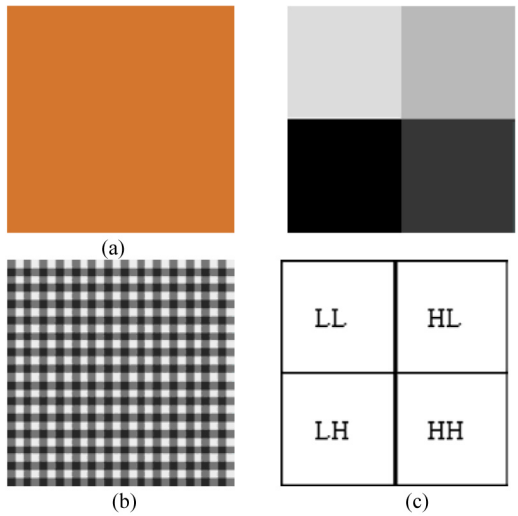

Fig. 5. Efficiency of representing Bayer pattern mosaic image in wavelet domain: (a) a uniform color image; (b) Bayer mosaic image; (c) 2-D wavelet coefficients. (Color version available online at http://ieeexplore.ieee.org.)

This linear combination of R, G, and B of rational coefficients is an approximation of the Y (luminance) component of the NTSC YUV color space. Interestingly, it is also exactly the same as the luminance component of reversible color transform adopted by JPEG 2000 in its lossless mode.

To understand the physical meanings of the three high subbands (HH, HL, and LH) of a mosaic image, we use a model of mosaic images that was originally developed for the purpose of color demosaicking [2]. In this model, a Bayer mosaic image [see Fig. 6(b)] is viewed as a sum of two component images

$$\begin{array}{ccccc}
G_{0,0} & R_{0,1} & G_{0,2} & R_{0,3} & G_{0,4} \\
B_{1,0} & G_{1,1} & B_{1,2} & G_{1,3} & B_{1,4} \\
G_{2,0} & R_{2,1} & G_{2,2} & R_{2,3} & G_{2,4} \\
B_{3,0} & G_{3,1} & B_{3,2} & G_{3,3} & B_{3,4} \\
G_{4,0} & R_{4,1} & G_{4,2} & R_{4,3} & G_{4,4}
\end{array}$$

$$= \begin{array}{ccccc}
G_{0,0} & G_{0,1} & G_{0,2} & G_{0,3} & G_{0,4} \\
G_{1,0} & G_{1,1} & G_{1,2} & G_{1,3} & G_{1,4} \\
G_{2,0} & G_{2,1} & G_{2,2} & G_{2,3} & G_{2,4} \\
G_{3,0} & G_{3,1} & G_{3,2} & G_{3,3} & G_{3,4} \\
G_{4,0} & G_{4,1} & G_{4,2} & G_{4,3} & G_{4,4}
\end{array}$$

$$+ \begin{array}{ccccc}
0 & \alpha_{0,1} & 0 & \alpha_{0,3} & 0 \\
\beta_{1,0} & 0 & \beta_{1,2} & 0 & \beta_{1,4} \\
0 & \alpha_{2,1} & 0 & \alpha_{2,3} & 0 \\
\beta_{3,0} & 0 & \beta_{3,2} & 0 & \beta_{3,4} \\
0 & \alpha_{4,1} & 0 & \alpha_{4,3} & 0.
\end{array}$$

The first component image, as shown in Fig. 6(c), is the full resolution green (an approximation of luminance) channel. The

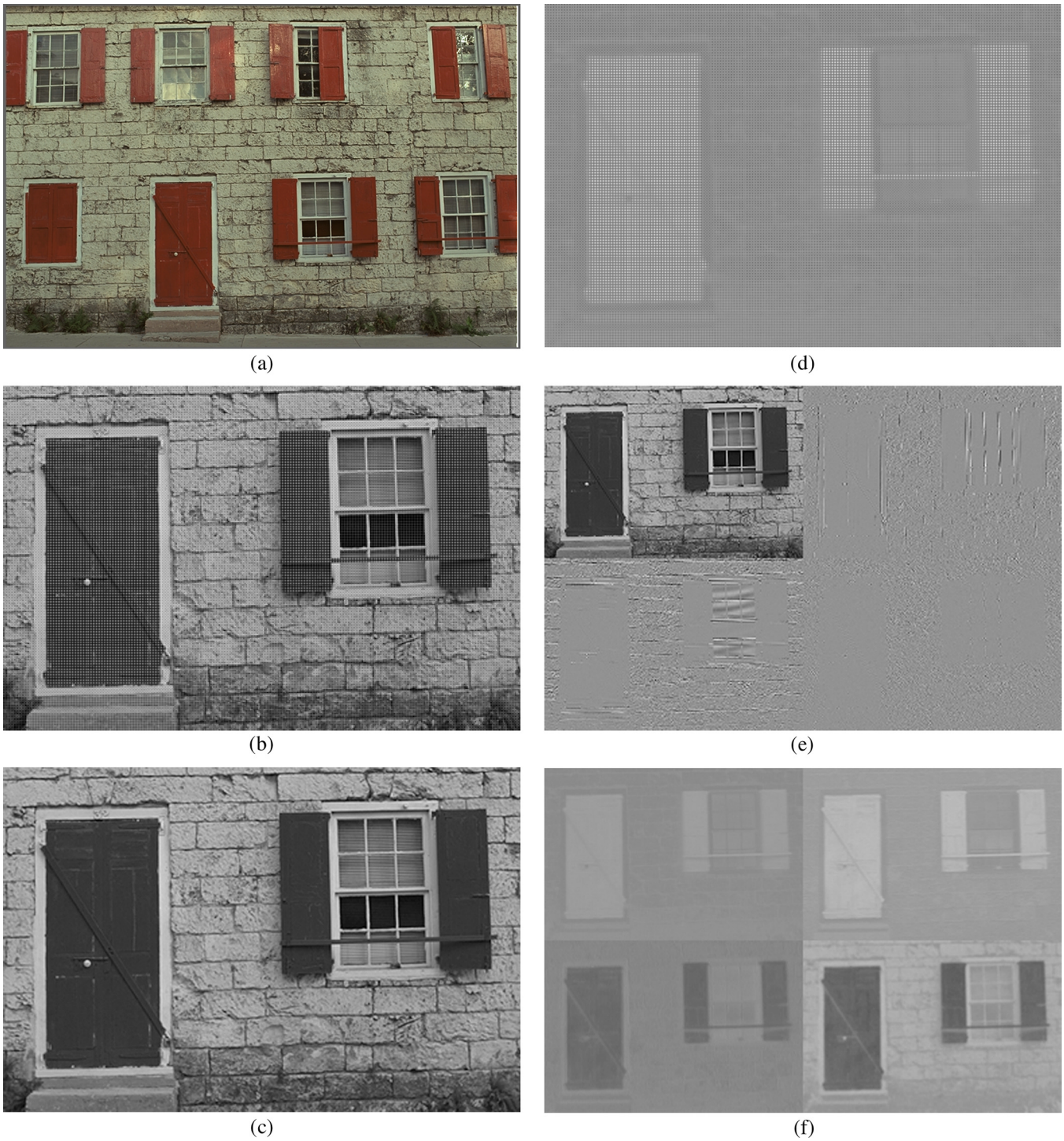

Fig. 6. Mosaic image model and effects of wavelet transform on Bayer mosaic images. (a) An original full-color image. (b) Bayer pattern mosaic image of (a). (c) The green channel of (a). (d) The checker board color difference signal of (a). The mid-gray (128) represents value 0. Note that image (b) is the sum of images (c) and (d). (e) One-level 2-D wavelet transform of the green channel (c). (f) One-level 2-D wavelet transform of the checker board color difference image (d). (Color version available online at http://ieeexplore.ieee.org.)

other component, as shown in Fig. 6(d), is a checker board sampled color difference (a representation of chrominance) image

$$\begin{aligned} \alpha_{(x,y)} &= R_{(x,y)} - G_{(x,y)}, \quad \text{for odd } x \text{ and } y \\ \beta_{(x,y)} &= B_{(x,y)} - G_{(x,y)}, \quad \text{for even } x \text{ and } y. \end{aligned} \tag{5}$$

As we argued in the preceeding section, the two color difference images $\boldsymbol{\alpha} = \mathbf{R} - \mathbf{G}$ and $\boldsymbol{\beta} = \mathbf{B} - \mathbf{G}$ are low-pass signals, because natural images mostly consist of pastoral (unsaturated) colors that have high correlation between the green and red/blue channels. An integer wavelet transform is approximately a linear operation, if we ignore the rounding. Applying wavelet transform directly to a mosaic image is, thus, equivalent to separately transforming the full resolution green channel [resulting in Fig. 6(e)] and the down sampled color difference image [resulting in Fig. 6(f)], and then summing up the results.

(g)

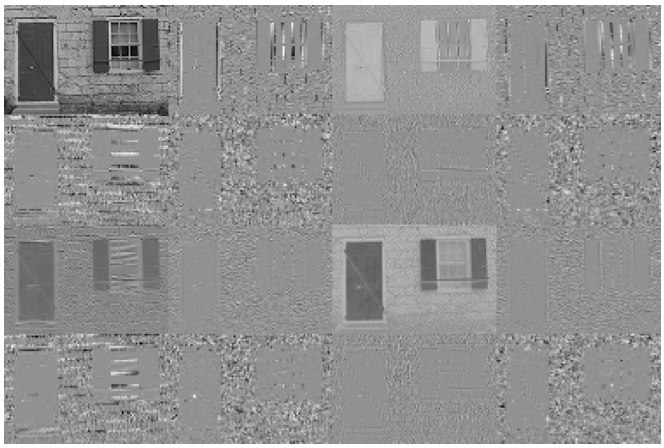

(h)

Fig. 6. (*Continued.*) Mosaic image model and effects of wavelet transform on Bayer mosaic images. (g) One-level 2-D wavelet transform of the mosaic image (b), which is approximately the sum of images (e) and (f). (h) Two-level 2-D Mallat packet decomposition of the mosaic image (b).

The net effect is the image in Fig. 6(g), whose characteristic is very different from a wavelet transformed grayscale image.

Now, let us analyze the outcome of such an operation. Applying the 2-D 5-3 HH high-pass filter

$$\mathbf{F}_{HH} = \mathbf{f}_H^T \mathbf{f}_H = \frac{1}{4}\begin{bmatrix} 1 & -2 & 1 \\ -2 & 4 & -2 \\ 1 & -2 & 1 \end{bmatrix} \tag{6}$$

to, say, position $G_{1,1}$, we have

$$x_{1,1} = \left[G_{1,1} - \frac{1}{2} \sum_{\substack{\{(0,1),(1,2)\} \\ \{(1,0),(2,1)\}}} G_{(x,y)} + \frac{1}{4} \sum_{\substack{\{(0,0),(0,2)\} \\ \{(2,0),(2,2)\}}} G_{(x,y)} \right] - \frac{1}{2}\left[(\alpha_{0,1} + \alpha_{2,1}) + (\beta_{1,0} + \beta_{1,2}) \right]. \tag{7}$$

The resulting HH subband can be viewed as a composition of a luminance component and a chrominance component. The first component is the detail signal of the usual HH subband of the green channel (luminance). The second component is low-pass filtered chrominance signal, in which the color difference image $\boldsymbol{\alpha} = \mathbf{R} - \mathbf{G}$ is averaged vertically and $\boldsymbol{\beta} = \mathbf{B} - \mathbf{G}$ averaged horizontally. Since color difference images $\boldsymbol{\alpha}$ and $\boldsymbol{\beta}$ are low-passed signals in the first place, the 5-3 high-pass filter actually (or quite counter intuitively) makes their HH response even smoother. In other words, the 5-3 high-pass filter has the effect of spectral decorrelation. As a result, in the HH subband of a Bayer mosaic image [see the HH subband of Fig. 6(g)], the details of the green channel [see the HH subband of Fig. 6(e)] are superimposed on a highly smoothed color difference signal [see the HH subband of Fig. 6(f)]. If we apply the 5-3 integer wavelet transform again to HH band [see Fig. 6(h)] we achieve greater energy compaction by further separating the green details from the smooth color difference signal.

Similar analysis can be carried out on LH/HL subbands. Applying the 2-D 5-3 LH high-pass filter

$$\mathbf{F}_{LH} = \mathbf{f}_H^T \mathbf{f}_L = \frac{1}{16}\begin{bmatrix} 1 & -2 & -6 & -2 & 1 \\ -2 & 4 & 12 & 4 & -2 \\ 1 & -2 & -6 & -2 & 1 \end{bmatrix} \tag{8}$$

to position $B_{1,2}$ yields

$$x_{1,2} = \left[\frac{3}{4} G_{1,2} - \frac{3}{8} \sum_{\left\{ \substack{(0,2) \\ (2,2)} \right\}} G_{(x,y)} + \frac{1}{4} \sum_{\{(1,1),(1,3)\}} G_{(x,y)} - \frac{1}{8} \sum_{\left\{ \substack{(0,1),(0,3) \\ (1,0),(1,4) \\ (2,1),(2,3)} \right\}} G_{(x,y)} + \frac{1}{16} \sum_{\left\{ \substack{(0,0),(0,4) \\ (2,0),(2,4)} \right\}} G_{(x,y)} \right] + \left[\left(-\frac{1}{8}\beta_{1,0} + \frac{3}{4}\beta_{1,2} - \frac{1}{8}\beta_{1,4} \right) - \frac{1}{8} \sum_{\left\{ \substack{(0,2),(0,3) \\ (2,1),(2,3)} \right\}} \alpha_{(x,y)} \right]. \tag{9}$$

Like the HH subband, the LH subband also consists of luminance and chrominance components. The luminance component is the detail signal of the usual LH subband of the green channel. The chrominance component is somewhat intricate, having two subcomponents: the smoothed color difference signal $\boldsymbol{\alpha} = \mathbf{R} - \mathbf{G}$ (the average of a four neighbor window), and a horizontally filtered signal $\boldsymbol{\beta} = \mathbf{B} - \mathbf{G}$ by filter $H(f) = 3/4 - 1/4\cos(2\pi f)$. In terms of contributions to the energy of the LH subband, the luminance component dominates since there is a significant amount of attenuation to the chrominance component.

The signal composition of the HL subband is analogous to that of the LH subband. It contains detail signal of the usual HL subband of the green channel, plus a smoothed $\boldsymbol{\beta}$ signal in a 2-D window and a vertically filtered $\boldsymbol{\alpha}$ signal using $H(f)$.

The analysis above reveals that all four subbands LL, HL, LH, and HH contain low-frequency components of either chrominance or luminance signals, as being evident in Fig. 6(g). The next natural step is to decompose these four subbands further to better pack the signal energy. The resulting sixteen subbands are shown in Fig. 6(h). The $LL0$ subband contains down sampled luminance information, while the energy of the chrominance signals is packed into the $LL1$, $LL2$, and $LL3$ subbands. The other twelve subbands, representing the much of image details in both luminance and chrominance, now become discontinuous signals of low amplitude very much like the

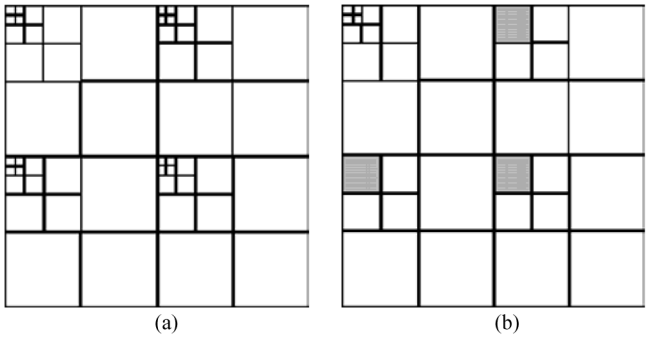

Fig. 7. Wavelet Decompositions. (a) Five-level of Mallat packet decomposition. (b) The decomposition closest to (a) that is realizable by JPEG 2000 decomposition options.

high-frequency wavelet subbands of normal continuous-tone images. Therefore, they should not be decomposed any further. Based on these observations, we introduce, for the purpose of maximum energy packing of mosaic images, a so-called Mallat packet decomposition as depicted in Fig. 7(a). It consists of a packet of four Mallat decompositions in $LL0$, $LL1$, $LL2$, and $LL3$ subbands, respectively.

We have also experimented with many other reversible integer wavelet filters in the Mallat packet for lossless compression of color mosaic images. In particular, we compare the energy packing capabilities of the popular 5/3, 9/7M, 5/11-C [10] and the simplest Haar filters on mosaic images. To evaluate these integer filters we tabulate in Table IV the self-entropies achieved by them after the five-level Mallat packet decomposition. These entropy results show that all integer wavelets, with exception of Haar wavelet that is about 4% worse, perform virtually the same. Furthermore, we investigated the combination of different filters at different decomposition levels of Mallat packet. In column six of Table IV the results are obtained by applying 9/7M filter in first level decomposition [Fig. 6(g)] and followed by the 5/3 filter in the other four levels [Fig. 7(a)]. Column seven lists the results for the combination of the 5/11C filter in first level and the 5/3 filter in other levels.

As for continuous-tone images, the wavelet transform does not generate i.i.d. coefficients on mosaic images. Higher lossless compression of mosaic images can be achieved by context modeling and adaptive arithmetic coding. We code the coefficients of Mallat packet transform using the high-order context-based entropy coding technique ECECOW [11]. The lossless bit rates of different integer wavelets when coded by ECECOW are listed in Table V.

TABLE IV
SELF-ENTROPY OF WAVELET COEFFICIENTS OF THE FIVE-LEVEL MALLAT PACKET DECOMPOSITION FOR DIFFERENT WAVELET FILTERS ON MOSAIC IMAGES

	Wavelet Transform					
Image	Haar	53	97M	5/11C	53+97M	53+5/11C
Woman	5.392	5.153	5.158	5.154	**5.121**	5.128
Bike	5.480	5.275	5.288	5.287	**5.255**	5.259
Monarch	5.120	4.697	4.672	**4.661**	4.694	4.689
Wall	6.003	5.858	5.895	5.883	**5.847**	5.85
Boat	5.561	5.355	5.370	5.364	**5.335**	5.338
Windows	6.189	5.956	5.985	5.983	**5.951**	5.955
Landscape	6.570	6.406	6.444	6.437	**6.400**	6.405
Fence	5.279	5.068	5.102	5.092	**5.067**	**5.067**
Lighthouse	5.396	5.213	5.254	5.240	5.215	**5.212**
Average	5.666	5.442	5.463	5.456	**5.432**	5.434

TABLE V
LOSSLESS BIT RATES OF MOSAIC IMAGES BY ECECOW FOR DIFFERENT INTEGER WAVELET TRANSFORMS

	Wavelet Transform					
Image	Haar	53	97M	5/11C	53+97M	53+5/11C
Woman	4.881	4.717	4.720	4.723	**4.699**	4.700
Bike	5.048	4.863	4.867	4.874	**4.847**	4.849
Monarch	4.627	4.285	4.255	**4.245**	4.283	4.277
Wall	5.632	**5.524**	5.56	5.561	5.527	5.525
Boat	5.075	4.898	4.907	4.903	4.88	**4.877**
Windows	5.887	5.678	5.699	5.703	**5.674**	**5.674**
Landscape	6.287	6.157	6.178	6.186	**6.154**	6.155
Fence	4.852	**4.678**	4.695	4.698	**4.678**	**4.678**
Lighthouse	4.905	**4.772**	4.803	4.795	4.777	**4.772**
Average	5.244	5.064	5.076	5.076	5.058	**5.056**

V. FAST CONTEXT-BASED COEFFICIENT CODING

Given the capability of integer wavelets in packing energy of mosaic images one can certainly use JPEG 2000 standard directly for lossless coding of mosaic images, using the options of 5-3 integer wavelet and the SPACL decomposition [two-level SPACL is equivalent to wavelet packet in Fig. 6(h)]. However, JPEG 2000 is not the best solution for this application in terms of either compression performance or low complexity. It has two disadvantages. First, JPEG 2000 does not support Mallat packet [Fig. 7(a)] as we proposed in the proceeding section. The closet decomposition that can be realized by JPEG 2000 VM8.0 is the one shown in Fig. 7(b), which is obtained by rather tedious decomposition option setting "-Fdecomp 31 -Fgen_decomp 11 100 011 000 110 001."

Second, and more importantly, the entropy coding module of JPEG 2000 is not suitable for Mallat packet. The three subbands shaded in Fig. 7(b) of Bayer pattern mosaic images tend to be smooth, not like the LH, HL, and HH subbands of full-resolution continuous-tone images. This property makes the context model of EBCOT [12] for high-frequency subbands ineffective. Furthermore, the entropy coding technique of JPEG 2000 is computationally expensive.

Aiming for on-camera real-time lossless encoding of mosaic images at lower computational complexity, we propose a much simpler and hardware-oriented entropy coding solution. Our design goal is to meet the requirements of low cost, longer battery life (requiring low-power consumption) and short shutter lag (requiring high-codec throughput), which are highly desirable features of digital cameras.

First, consider entropy coding of the twelve high-frequency subbands generated by the 2-D two-level Mallat packet transform. Since the lifting scheme of the integer wavelet essentially performs linear prediction operations on pixels [13], the wavelet coefficients in the high-frequency subbands can be viewed as prediction residuals. It is well known in signal compression that the distribution of prediction errors is approximately Laplacian. This fact and our above-mentioned design objective make Golomb code a natural choice for the entropy coding of high-frequency subbands. The Golomb code is a low-complexity adaptive entropy coding technique and is yet optimal for geometrical distribution [14].

The Golomb code operates on random variables of positive integer values. A positive integer x is coded in two parts: The quotient $s = \lfloor x/\lambda \rfloor$ and the remainder $r = x \bmod \lambda$, where λ is the so-called Golomb parameter which is itself also a positive

integer. The code stream of x is the concatenation of the unary code of s and the binary code of r. Obviously, the Golomb parameter λ determines the code length of x. The Golomb code affords a very simple implementation if its parameter is an integer power of two, $\lambda = 2^t$, $t \geq 0$. In this case, the code of x has a quotient part that is generated by simply right-shifting x by t bits, and the remainder is just the t least significant bits of x. This special form of Golomb code is also known as the Rice code.

Next, we develop a simple context-based Rice coding scheme to compress integer wavelet coefficients. Coefficients in each subband are coded in raster scan order from left to right and top to bottom. A wavelet coefficient X is split into its sign and magnitude $|X|$. The sign of X is kept uncoded and $|X|$ is represented in Rice code. The key to the performance of Rice code is the choice of the parameter λ. The flexibility of changing the value of λ per source symbol on the fly makes Rice code adaptive to the changing statistics of the input signal. Specifically for lossless wavelet compression of mosaic images, the wavelet coefficients are not i.i.d. because wavelet transform clusters coefficients in the spatial domain by magnitudes. It can be readily observed from Fig. 6(h) that large wavelet coefficients tend to occur in vicinity of edges, and conversely small coefficients form large contiguous blocks. To exploit this memory structure of the source, we associate the current wavelet coefficient X, which is the random variable to be coded, with the L-shaped neighborhood or context of X:

$$\begin{matrix} NW & N & NE \\ W & C & \end{matrix}$$

and we define the energy of the neighborhood by

$$\Delta = |X_w| + |X_n| + \frac{1}{2}\left(|X_{nw}| + |X_{ne}|\right). \tag{10}$$

Denote by $L(X;\lambda|\Delta)$ the Rice code length given context Δ and parameter λ. Having chosen the Rice code for its operational advantage, we still have the room to optimize λ with respect to context Δ to minimize the code length $L(X;\lambda|\Delta)$. The underlying optimization problem is to determine the optimal value of λ

$$\breve{\lambda} = \arg\min_{\lambda} L\left(X;\lambda|\Delta\right). \tag{11}$$

Note that Δ increases in the variance of X, if X is drawn from a process, which is stationary, zero-mean, and of unimodal marginal distribution in the window of the context Δ. This is the case for high-frequency wavelet coefficients whose distribution is known to be Laplacian. Consequently, $\breve{\lambda}$ is monotonically nondecreasing in Δ. Since the Rice parameter has integer values, the distinct values of $\breve{\lambda}$ partition the interval of the Δ values into contiguous subintervals. This property reduces the optimization problem of (9) to the following optimal scalar context quantization problem:

$$\breve{\mathbf{Q}} = \min_{\mathbf{Q}} \sum_{k=0}^{K} L\left(X;\lambda = K|Q(\Delta) = k\right) \tag{12}$$

where $\mathbf{Q}$ is a scalar quantizer of random variable Δ and K is the maximum number of Rice parameters to be used. The design of the optimal context quantizer $\breve{\mathbf{Q}}$ can be done via dynamic programming [15]. Although it is possible to compute the image-dependent optimal context quantizer $\breve{\mathbf{Q}}$ to minimize the Rice code length for an input image, this approach is clearly impractical for most digital camera applications. However, one can compute $\breve{\mathbf{Q}}$ in an offline design process using a training set that provides sample statistics of the joint distribution of (X, Δ). The training set(s) should be chosen for given integer wavelet transform, given CCD sensor, and may also be with respect to different types of scenes, but we found empirically that the following simple partition of Δ

$$\mathbf{Q} = \{0, 2, 8, 32, 64, 128, 256, 512, 1024, +\infty\} \tag{13}$$

works well on 8-bit mosaic images (within less than 2% from the minimum Rice code length achieved by $\breve{\mathbf{Q}}$ computed by dynamic programming).

For the four smooth subbands: $LL1$, $LL2$, $LL3$, and $LL4$, a simple DPCM coding is employed first. For current coefficient X_i at position C, a linear prediction is performed as

$$e_i = X_i - \left[\frac{1}{2}(X_n + X_w) + \frac{1}{4}(X_{ne} - X_{nw})\right]. \tag{14}$$

After prediction, the prediction residual e_i is treated the same as those coefficients in high subbands. The e_i is mapped from signed integer into no-negative integer E_i by

$$E_i = \begin{cases} 2e_i, & e_i \geq 0 \\ -2e_i - 1, & e_i < 0. \end{cases} \tag{15}$$

A simple context for current value E_i is formed as

$$\Delta_i = E_w + E_n + \frac{1}{2}(E_{nw} + E_{ne}). \tag{16}$$

The context value Δ_i is quantized by preset thresholds to determine the Golomb–Rice variable λ_i for E_i

$$\lambda_i = \arg_k\{Q_k \leq \Delta_i < Q_{k+1}\}. \tag{17}$$

VI. Experimental Results

We implemented the simple entropy coding technique described above and evaluated its performance when coupled with the 5-3 integer wavelet. In our experiments, we simulated color mosaic images by subsampling some typical color images drawn from the ISO JPEG test set [Woman, Bike (2048 × 2560)] and the Kodak set (768 × 512) [some examples are given in Fig. 1(b)], and interleaving the samples according to the Bayer pattern.

Table VI presents the lossless bit rates of the proposed method in comparison with JPEG-LS and the lossless mode of JPEG 2000 when applied directly to raw mosaic images of Bayer pattern. JPEG 2000 was tested for different decomposition schemes: default Mallat, SPACL, Hybrid [as shown in Fig. 7(b)], and the corresponding results are listed in Table VI (columns three to five). The proposed method, despite its

TABLE VI
LOSSLESS BIT RATES OF MOSAIC IMAGES BY JPEG-LS, JPEG 2000, AND PROPOSED METHOD

		JPEG 2000			
Image	**JPEG-LS**	Default	SPACL	Hybrid	**Proposed**
Woman	5.592	4.943	4.913	4.900	4.876
Bike	5.791	5.045	5.035	5.031	4.908
Monarch	7.216	4.893	4.528	4.456	4.377
Wall	6.398	5.809	5.762	5.746	5.65
Boat	5.862	5.207	5.117	5.085	5.028
Windows	6.286	5.895	5.892	5.887	5.725
Landscape	6.735	6.368	6.387	6.384	6.243
Fence	5.47	4.907	4.867	4.846	4.823
Lighthouse	5.469	5.034	4.958	4.943	4.867
Average	**6.091**	**5.345**	**5.273**	**5.253**	**5.166**

simplicity, outperforms all other methods on every single test image.

Note that the average bit rate of the proposed interleaved compression method is also lower than the best de-interleaved coding results of JPEG-LS in Table III, although JPEG-LS uses on-line context modeling techniques of higher complexity.

Comparing Tables V and VI, we see that the performance gap between the simple Rice code and computationally intensive ECECOW technique is only about 2%, while the former is more than six times faster than the latter. The encoder and decoder throughputs of the proposed method are more than four times higher than JPEG 2000 and 90% higher than JPEG-LS.

VII. CONCLUSION

Various techniques for lossless coding of raw color mosaic images generated by CCD cameras of Bayer pattern were investigated. It turned out that the integer wavelet transform is ideally suited to the task, by offering efficient energy packing in both image and color spaces. A fast and practical codec for lossless compression of mosaic images was developed.

JPEG 2000 standard (in its lossless mode) can be conveniently applied to lossless compression of color mosaic images. As a simpler and faster alternative we have also developed a lossless mosaic image codec based on integer Mallat packet transform and Rice code. This codec outperforms JPEG 2000 and JPEG-LS in both bit rate and speed.

REFERENCES

[1] B. Bayer, "Color Imaging Array," U.S. Patent 3 971 065.

[2] X. Wu and N. Zhang, "Primary-consistent soft-decision color demosaicking for digital cameras," *IEEE Trans. Image Process.*, vol. 13, no. 9, pp. 1263–1274, Sep. 2004.

[3] K. Hisakazu, M. Shogo, T. Ishida, and T. Kuge, "Reversible conversion between interlaced and progressive scan formats and its efficient implementation," presented at the EUSIPCO Conf., Sep. 2002, Paper 448.

[4] C. C. Koh and S. K. Mitra, "Compression of Bayer color filter array data," in *Proc. Int. Conf. Image Processing*, vol. 2, Barcelona, Spain, Sept. 2003, pp. 255–258.

[5] *Information Technology—Lossless and Near-Lossless Compression of Continuous-Tone Still Images*, ISO FDIS 14 495-1(JPEG-LS), 1998.

[6] *JPEG 2000 Part I Final Draft International Standard*, 2000.

[7] D. R. Cok, "Signal Processing Method and Apparatus for Sampled Image Signals," U.S. Patent 4 630 307, 1987.

[8] R. H. Hibbard, "Apparatus and Method for Adaptively Interpolating a Full Color Image Utilizing Luminance Gradients," U.S. Patent 5 382 976, 1995.

[9] O. Rashkovskiy and W. Macy, "Method of Determining Missing Color Values for Pixels in a Color Filter Srray," U.S. Patent 6 181 376, 2001.

[10] M. D. Adams, "Reversible integer-to-integer wavelet transforms for image compression: performance evaluation and analysis," *IEEE Trans. Image Process.*, vol. 9, no. 6, pp. 1010–1024, Jun. 2000.

[11] X. Wu, "High-order context modeling and embedded conditional entropy coding of wavelet coefficients for image compression," in *Proc. 31st Asilomar Conf. Signals, System, and Computers*, Nov. 1997, pp. 1378–1382.

[12] D. Taubman, "High Performance Scalable Image Compression Width EBCOT," *IEEE Trans. Image Process.*, vol. 9, no. 7, pp. 1158–1170, Jul. 2000.

[13] A. Said and W. A. Pearlman, "An image multiresolution representation for lossless and lossy compression," *IEEE Trans. Image Process.*, vol. 5, no. 9, pp. 1303–1310, Sep. 1996.

[14] R. G. Gallager and D. C. Van Voorhis, "Optimal source code for geometrically distributed integer alphabets," *IEEE Trans. Inf. Theory*, vol. IT-21, no. 3, pp. 228–230, Mar. 1975.

[15] N. Zhang and X. Wu, "Lossless Compression of Color Mosaic Images," presented at the Int. Conf. Image Processing, Singapore, 2004.

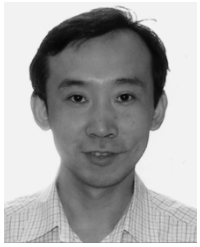

Ning Zhang received the B.E. and Ph.D. degrees in electrical engineering from Tsinghua University, Beijing, China, in 1994 and 2000, respectively.

He is currently a Research Associate with McMaster University, Hamilton, ON, Canada. His research interests include data compression, image processing, multimedia communication, and digital cinema.

Xiaolin Wu (M'88–SM'96) received the B.Sc. degree from Wuhan University, China, in 1982, and the Ph.D. degree from the University of Calgary, Calgary, AB, Canada, in 1988, both in computer science.

He is currently a Professor with the Department of Electrical and Computer Engineering, McMaster University, ON, Canada, where he holds the NSERC-DALSA Research Chair in Digital Cinema. His research interests include multimedia coding and communications, image processing, signal quantization and compression, and joint source-channel coding. He has published over 160 research papers and holds two patents in these fields.

Dr. Wu received the 2003 Nokia Visiting Fellowship, the 2000 Monsteds Fellowship, and the 1998 UWO Distinguished Research Professorship